Upper mantle anisotropy beneath the Seychelles microcontinent

J. O. S. Hammond,[1] J.-M. Kendall,[1,2] G. Rümpker,[3,4] J. Wookey,[1,2] N. Teanby,[1,5] P. Joseph,[6] T. Ryberg,[3] and G. Stuart[1]

Received 1 April 2005; revised 22 July 2005; accepted 12 August 2005; published 4 November 2005.

[1] The Seychelles plateau is a prime example of a microcontinent, yet mechanisms for its creation and evolution are poorly understood. Recently acquired teleseismic data from a deployment of 26 stations on 18 islands in the Seychelles are analyzed to study upper mantle seismic anisotropy using *SKS* splitting results. Strong microseismic noise is attenuated using a polarization filter. Results show significant variation in time delays (δt = 0.4–2.4 s) and smooth variations in orientation ($\phi = 15°–69°$, where ϕ is the polarization of the fast shear wave). The splitting results cannot be explained by simple asthenospheric flow associated with absolute plate motions. Recent work has suggested that anisotropy measurements for oceanic islands surrounding Africa can be explained by mantle flow due to plate motion in combination with density-driven flow associated with the African superswell. Such a mechanism explains our results only if there are lateral variations in the viscosity of the mantle. It has been suggested that the Seychelles are underlain by a mantle plume. Predictions of flow-induced anisotropy from plume-lithosphere interaction can explain our results with a plume possibly impinging beneath the plateau. Finally, we consider lithospheric anisotropy associated with rifting processes that formed the Seychelles. The large variation in the magnitude of shear wave splitting over short distances suggests a shallow source of anisotropy. Fast directions align parallel to an area of transform faulting in the Amirantes. Farther from this area the orientation of anisotropy aligns in similar directions as plate motions. This supports suggestions of transpressive deformation during the opening of the Mascarene basin.

Citation: Hammond, J. O. S., J.-M. Kendall, G. Rümpker, J. Wookey, N. Teanby, P. Joseph, T. Ryberg, and G. Stuart (2005), Upper mantle anisotropy beneath the Seychelles microcontinent, *J. Geophys. Res.*, *110*, B11401, doi:10.1029/2005JB003757.

1. Introduction

[2] The spectacular granite outcrops of the Seychelles Islands in the Indian Ocean, were cited as evidence for continental drift early in the last century [*Wegener*, 1924]. Despite this, mechanisms for isolating such a microcontinent are still poorly understood. Few investigations of mantle flow beneath this region have been carried out. What information we have comes from global studies [e.g., *Montelli et al.*, 2004; *Debayle et al.*, 2005] which provide a broad picture of mantle dynamics beneath the Indian ocean. With this study we aim to better constrain the dominant mechanism for upper mantle anisotropy which will aid in our understanding of mantle dynamics beneath the region. We consider the potential influence of the African superswell [*Behn et al.*, 2004], a plume like upwelling beneath the region [*Montelli et al.*, 2004] and fossil anisotropy preserved in the lithosphere.

[3] The granites of the Seychelles microcontinent were emplaced ~750 Ma, during the late Precambrian [*Miller and Mudie*, 1961; *Wasserburg et al.*, 1963; *Plummer*, 1995; *Tucker et al.*, 2001]. Thermally induced rifting in the Somali basin and transform rifting along the Davies fracture zone (Figure 1) began in the late Permian (~225 Ma), with Gondwana breaking into East and West Gondwana ~160 Ma to form the Somali basin, and ceased spreading ~115 Ma [*Plummer and Belle*, 1995]. The Seychelles then underwent two more stages of rifting to isolate it from Madagascar and India. Between ~95 Ma and ~84 Ma rifting separated Seychelles/India from Madagascar. An initial period of transform rifting moved the Seychelles/India block northward [*Plummer and Belle*, 1995; *Plummer*, 1996]. At ~84 Ma oceanic crust started to form in the Mascarene basin [*Schlich*, 1982], causing a rotation of the Seychelles/India landmass. This continued until ~65 Ma when new rifting severed the Seychelles from India forming

[1]School of Earth and Environment, Earth Science, University of Leeds, Leeds, UK.
[2]Now at Department of Earth Sciences, University of Bristol, Bristol, UK.
[3]GeoForschungsZentrum Potsdam, Potsdam, Germany.
[4]Arbeitsbereich Geophysik, Johann Wolfgang Goethe-Universitat, Frankfurt am Main, Germany.
[5]Atmospheric, Oceanic and Planetary Physics, University of Oxford, Clarendon Laboratory, Oxford, UK.
[6]Seychelles National Oil Company, Victoria, Mahé, Seychelles.

0148-0227/05/2005JB003757$09.00

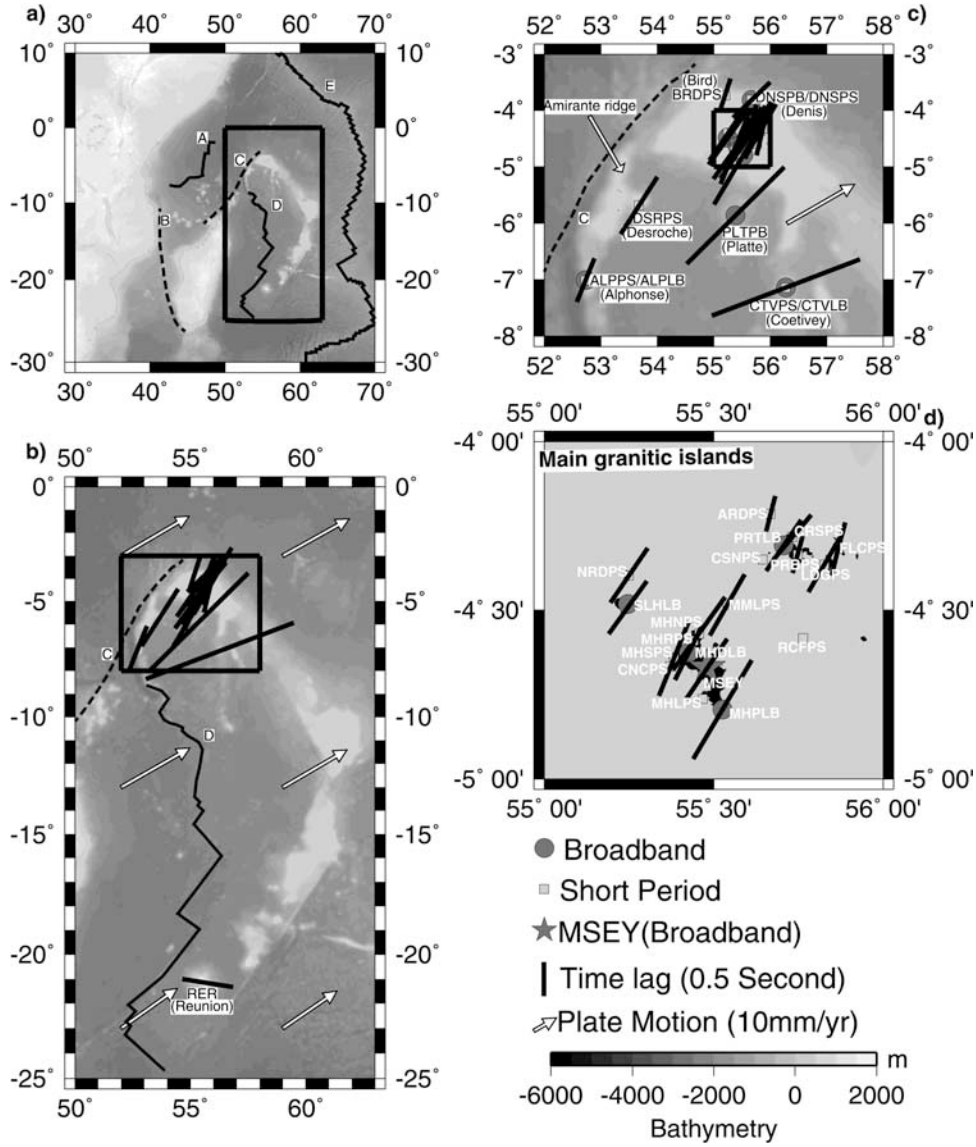

Figure 1. (a) Regional setting of the Seychelles. Ridge locations are from *Müller et al.* [1997]. A, extinct ridge in the Somali Basin; B, Davies fracture zone [*McCall*, 1997]; C, transform fault near the Amirante ridge [*Plummer*, 1996]; D, extinct ridge in the Mascarene Basin; and E, active Carlsberg Ridge. Shear wave splitting results are shown for seismic stations in the Seychelles, including (b) Reunion, (c) across the Seychelles array, and (d) the inner islands (Mahé, Praslin, and satellite islands). The orientation of the solid lines shows the fast shear wave polarization direction (ϕ), and the length of the line is proportional to the magnitude of the splitting (δt). Circles mark broadband stations, squares mark short-period stations, and the star marks the permanent IRIS station MSEY (note MHRPS moved to MHNPS on 16 July 2003). Bathymetry [*Smith and Sandwell*, 1997] and topography [*Hastings and Dunbar*, 1999] are also shown. White arrows show direction of absolute plate motion as estimated by *Kreemer et al.* [2003]. Result for MSEY is from *Barruol and Ben Ismail* [2001], and RER is from *Behn et al.* [2004].

the currently active Carlsberg Ridge (Figure 1). The rift jump coincided with the maximum output of the Deccan traps [*Duncan and Pyle*, 1988], and volcanics found on the Seychelles Plateau have also been linked with this event [*Plummer*, 1995]. This has led to suggestions that the initiation of the Reunion plume caused rifting to jump to its current location [*Müller et al.*, 2001; *Gaina et al.*, 2003].

[4] In 2003 a major seismic experiment was carried out to study the Seychelles-Laxmi ridge and the Seychelles microcontinent [*Collier et al.*, 2004]. The first stage of the experiment involved a marine survey, collecting controlled source data across the Seychelles-Laxmi continental margins. In phase 2, 26 stations were deployed across the Seychelles from February 2003 to January 2004, to record teleseismic earthquakes (Figure 1). Here we present a shear wave splitting analysis of core phases (*SKS*, *SKKS*) from the passive part of the seismic experiment in order to determine upper mantle seismic anisotropy and hence interpret dynamic processes in the mantle beneath the Seychelles.

Table 1. Earthquakes Used to Estimate Shear Wave Splitting

Event	Date	Time	Latitude	Longitude	Depth, km
1	6 Mar 2003	1024:42	−23.60	−175.81	10
2	10 Mar 2003	1002:41	−28.07	−177.68	146
3	14 Mar 2003	1254:12	−17.42	−175.18	274
4	31 Mar 2003	0106:53	−6.18	151.43	46
5	26 May 2003	0924:33	38.35	141.57	68
6	21 Jul 2003	1353:59	−5.51	148.96	190
7	25 Jul 2003	0937:49	−1.51	149.64	50
8	27 Jul 2003	0625:33	47.18	139.22	481
9	28 Aug 2003	0448:20	−49.76	−114.66	10
10	25 Sep 2003	1950:08	42.17	143.72	33
11	17 Oct 2003	1019:07	−5.50	154.12	133
12	12 Nov 2003	0826:46	33.63	137.02	391
13	25 Nov 2003	2019:46	−5.52	150.88	33
14	27 Dec 2003	1019:07	−22.01	169.61	10

[5] Shear wave splitting in core phases is an indicator of the magnitude and orientation of seismic anisotropy (the variation of seismic wave speed with direction) in the mantle. A wave such as *SKS*, which has passed through the liquid outer core as a *P* wave, is radially polarized upon reentering the mantle as an *S* wave. If this wave encounters an anisotropic region on its way to the surface it will be split into two quasi shear waves. These waves will be polarized orthogonally to one another and will propagate at different velocities. The time lag (δt) between the fast and slow shear waves and the polarization of the fast shear wave (ϕ) is used to characterize anisotropy beneath a station.

[6] In most studies the main cause of anisotropy in the upper mantle is assumed to be the lattice-preferred orientation (LPO) of olivine where the olivine fast axis (*a* axis) aligns in the direction of upper mantle flow [*Babuska and Cara*, 1991; *Mainprice et al.*, 2000]. Anisotropy decreases rapidly below ~250 km [e.g., *Gung et al.* 2003] and this decrease has been attributed to a change in deformation regime from dislocation creep to diffusion creep [*Karato*, 1992] or a change in the LPO of olivine, where the olivine *c* axis aligns in the direction of upper mantle flow below 250 km [*Mainprice et al.*, 2005]. As a result shear wave splitting can provide direct information about the stress regime from current forces, such as seafloor spreading, and accumulated strain due to previous deformation events which have ''frozen'' a source of anisotropy into the lithosphere beneath a seismic station. It is the aim of this study to see if mantle anisotropy beneath the Seychelles offers any insights into the dynamic history of the region.

2. Data Set

[7] Eight broadband and 18 short-period, three-component, seismic stations were deployed in the Seychelles from February 2003 to January 2004 (Figure 1). The broadband stations primarily consisted of Guralp CMG3T seismometers and Nanometrics Orion data loggers. Three of the broadband stations had Guralp CMG40T sensors, ALPLB (with a Nanometrics Orion data logger), and PLTPB and DNSPB (with Earth data data loggers). The short-period stations used Mark L4C-3D seismometers and Earth data data loggers. All stations recorded with a sampling rate of 20 Hz.

[8] The majority of the stations were located on the granitic islands of Mahé and Praslin and their satellite islands. More distant sites were situated on coral islands on the edge of or beyond the Seychelles plateau (Figure 1). The aperture of the resulting triangular array was on the order of 500 km.

[9] During the period of deployment 239 earthquakes >5.8 M_b were recorded, of which 143 fell in to a suitable range for analyzing SKS/SKKS phases (85°–140°). Of these events 14 were of sufficient quality for shear wave splitting analysis (Table 1).

3. Data Processing

3.1. Shear Wave Splitting Analysis

[10] We estimate shear wave splitting in *SKS*/*SKKS* phases using the semiautomated approach of *Teanby et al.* [2004], which is based on the methodology of *Silver and Chan* [1991]. For *SKS* waves, elliptical particle motion and energy on the transverse component are evidence of shear wave splitting. We rotate and time shift the horizontal components to minimize the second eigenvalue of the covariance matrix for particle motion of a time window around the shear wave arrival. This corresponds to linearizing the particle motion, and usually reducing the transverse component energy (assuming the incoming *SKS* wave is radially polarized before entering the anisotropic medium). 100 splitting measurements are made for 100 different windows selected around the relevant core phase. Cluster analysis is then used to find the most stable splitting parameters [*Teanby et al.*, 2004]. Figure 2 shows an example of this analysis for an event recorded at the permanent IRIS station MSEY, located on the island of Mahé (Figure 1).

3.2. Polarization Analysis

[11] A necessary preprocessing step was a check of the orientation of the horizontal components at each seismic station. It is assumed that the stations have been aligned with the horizontal components north-south and east-west. Station misalignment will introduce an artifact into shear wave splitting results, a $\delta\phi°$ misalignment causes a $\delta\phi°$ systematic error in the estimated polarization of the fast shear wave. Principal component analysis was used to calculate the direction of *P* wave particle motion. The average systematic difference between these directions and the receiver-source azimuth for all events recorded at a station were used to estimate the station misalignment correction and an associated standard error (Table 2). Most stations had a small misalignment (<5°). Three stations had alignment errors greater than 5° (CRSPS 20.0°, DNSPB 7.0° and NRDPS 11.1°). These misalignments were removed from the measured anisotropy a posteriori.

3.3. Polarization Filtering

[12] Many of the stations were located on small islands and microseismic noise caused a significant problem, particularly during May–October when the SE trades cover the region [*Walsh*, 1984]. During this time wind speeds increase by a factor of three which result in the peak-peak amplitude of microseismic noise increasing by a factor of five. Data-adaptive polarization filters, developed by *Du et al.* [2000] and similar to those used by *Reading et al.* [2001], were employed to improve the signal-to-noise ratio. The filters

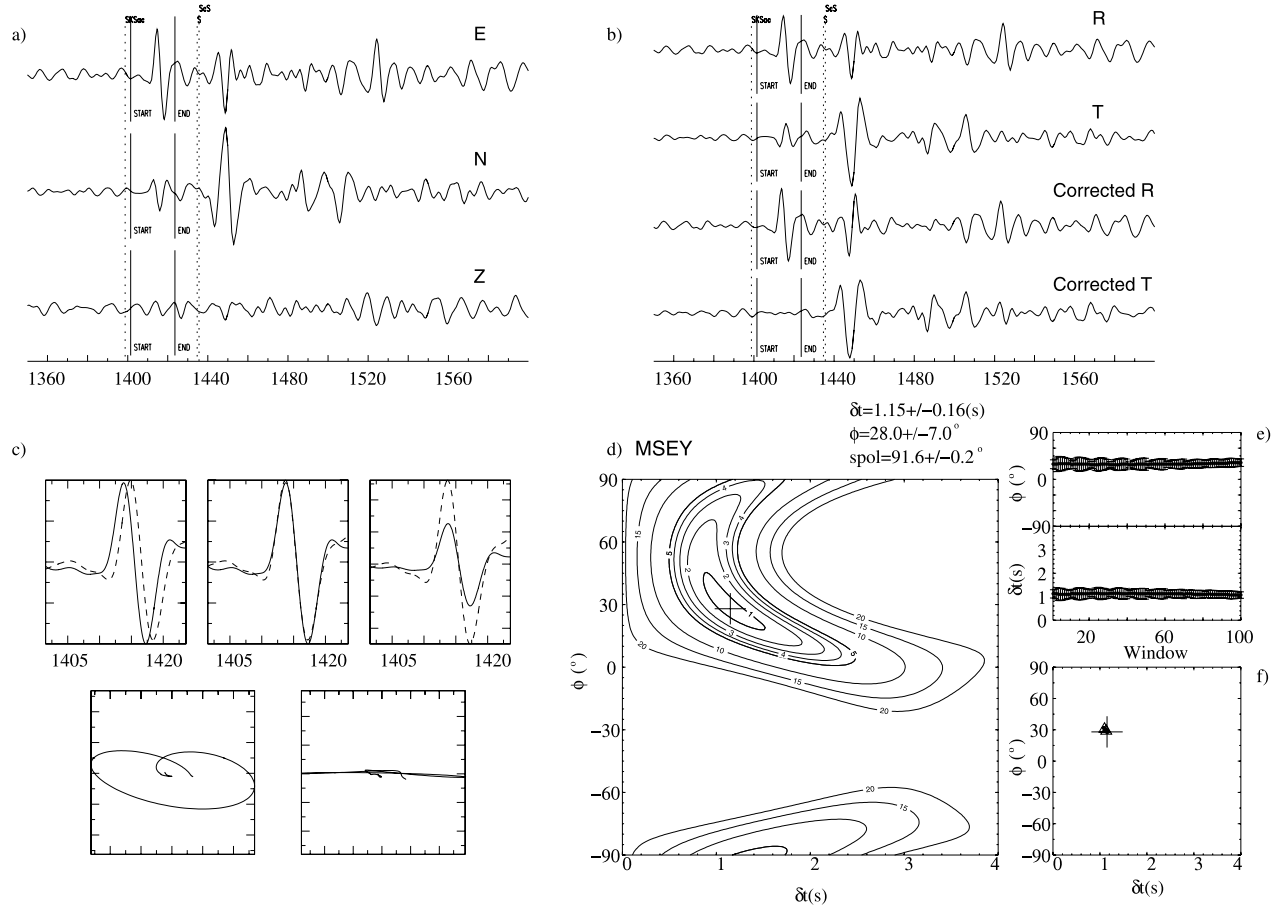

Figure 2. Splitting analysis performed at MSEY on an event recorded on 5 April 1999, 1108:04:0 UT. New Britain Region, Papua New Guinea. (a) Original traces (E, N, Z). (b) Traces rotated into R and T directions before and after the anisotropy correction. R component is the initial shear wave polarization before entering the anisotropic region. In a 1-D Earth, R and T will be the radial and transverse components. Energy on the corrected transverse trace should be minimized in the analysis window. (c) Top traces show the fast/slow shear waveforms for uncorrected (left) and corrected (middle (normalized)/right (real amplitudes)) seismograms. The bottom panels show the particle motion for uncorrected (left) and corrected (right) seismograms. A good result will show similar fast/slow shear waveforms and any elliptical particle motion will have been linearized. (d) Results of the grid search over δt and ϕ. The optimum splitting parameters are represented by the cross, and the first surrounding contour denotes the 95% confidence region. (e) Measurements of δt and ϕ obtained from 100 different analysis windows plotted against window number. A stable result will have a similar solution independent of analysis window. (f) Cluster analysis of δt and ϕ obtained from 100 different analysis windows. A good result will have solutions clustered in one area. All data have been band-pass filtered between 0.05 and 0.3 Hz. The best fitting shear wave splitting parameters for this event is a fast direction of 28° ± 7° and a time lag of 1.15 s ± 0.16 s.

are designed to enhance signals with linear or elliptical polarization and thus to suppress more random noise.

[13] They use the 3 × 3 spectral density matrix (**S**) from three-component data calculated using spectral multitapers [*Park et al.*, 1987]. Each component of the seismogram is multitapered by K leakage resistant tapers, which results in K time series. **S** can then be constructed from these K time series:

$$\mathbf{S}(\omega) = \frac{1}{K}\mathbf{M}^{\dagger}(\omega)\cdot\mathbf{M}(\omega), \tag{1}$$

where

$$\mathbf{M}(\omega) = \begin{vmatrix} z_0^{(1)}(\omega) & z_0^{(2)}(\omega) & z_0^{(3)}(\omega) \\ z_1^{(1)}(\omega) & z_1^{(2)}(\omega) & z_1^{(3)}(\omega) \\ \vdots & \vdots & \vdots \\ z_{K-1}^{(1)}(\omega) & z_{K-1}^{(2)}(\omega) & z_{K-1}^{(3)}(\omega) \end{vmatrix} \tag{2}$$

and $z_j^{(i)}(\omega)$ is the eigenspectra of component i and eigentaper j and the dagger denotes the Hermitian adjoint. This results in a spectral density matrix (**S**) with a very smooth spectrum. The matrix **S** can be expressed in terms of its

Table 2. Misalignment of Seismic Stations[a]

Station	Misalignment, deg	Standard Error, deg
ALPLB (Alphonse)	−3.5	1.0
ARDPS (Aride)	4.3	1.6
BRDPS (Bird)	0.0	0.3
CRSPS (Curieuse)	−20.0	2.6
CTVPS (Coetivy)	0.1	0.9
DNSPB (Denis)	7.0	2.9
DSRPS (Desroches)	4.4	0.9
FLCPS (Felicite)	0.8	2.0
LDGPS (La Digue)	−1.1	1.8
MHDLB (Mahé)	0.3	1.2
MHNPS (Mahé)	3.4	2.1
MHPLB (Mahé)	2.4	0.8
MHSPS (Mahé)	2.7	2.2
MMLPS (Mahé)	3.5	2.9
NRDPS (Île Du Nord)	11.1	3.4
PLTPB (Île Platte)	2.0	3.6
PRBPS (Praslin)	2.1	2.5
PRTLB (Praslin)	−3.5	1.2
SLHLB (Silhouette)	−4.9	1.0

[a]Calculated using principal component analysis to determine *P* wave particle motion.

eigenvalues and eigenvectors. A large degree of polarization is observed where **S** has a dominant eigenvalue and associated eigenvector. The degree of polarization ($P(\omega)$) is then given by

$$P = \frac{n\left(Tr\mathbf{S}^2\right) - \left(Tr\mathbf{S}\right)^2}{(n-1)\left(Tr\mathbf{S}\right)^2}, \tag{3}$$

where $Tr\mathbf{S}$ denotes the trace of the matrix **S**. P has a value of $0 \leq P \leq 1$ and it is this estimate of polarization which defines the filter in the frequency domain. P is raised to a power g to control the harshness of the filter. Filtering is then completed by multiplication in the frequency domain followed by an inverse Fourier transform back to the time domain. A sliding window is used to account for different arrivals on the seismogram differing in frequency content.

[14] However, microseismic noise can contain polarized signal [e.g., *Schulte-Pelkum et al.* 2004]. The filters account for this by analyzing **S** for a presignal noise window and using this information when constructing the filters from the spectral density matrix of the three-component data.

[15] The parameters which control the filter are the number of eigentapers used for the spectral analysis (K), a positive number that controls the level of rejection of polarized noise (g), the length of the presignal noise window and the length of the sliding window. K and g should be kept between 4 and 6 [*Du et al.*, 2000] and the sliding window should contain at least one complete wavelength of the signal of interest. *Du et al.* [2000] suggest that a longer time window is preferential, but in the case of shear waves a short time window may be desirable due to the contaminating effects of the *P* coda [*Wookey and Kendall*, 2004]. The presignal noise window is typically 3 times the sliding window. For a more detailed discussion on the polarization filters used in this study, see *Du et al.* [2000].

[16] To test the effects of the polarization filter, we consider an example splitting result from the permanent station MSEY, which has been studied previously by *Barruol and Ben Ismail* [2001] (Figure 2). Preevent noise taken from MSEY was multiplied by a factor (which varies depending on the desired level of microseismic noise) and added to these data, then filtered using the polarization filters, with parameters, $K = 4$, $g = 4$, sliding window of 20 s and noise window of 60 s. Shear wave splitting results are then compared before and after to assess the effect of the polarization filter (Figure 3). The results agree within error bounds, and the polarization filter brings the errors back to within acceptable limits ($\delta t < 0.4$ s, $\phi < 20°$).

[17] Signal-to-noise ratios between the *SKS* signal and the background noise are calculated using SNR = SKS_{amp}/BN_{amp}, where SNR is the signal-to-noise ratio, SKS_{amp} is the peak-peak amplitude of the *SKS* signal on the component where it has the smallest amplitude (usually the transverse component), and BN_{amp} is the peak-peak amplitude of the background noise surrounding the *SKS* arrival on the same component. The errors in the splitting analysis before and after polarization filtering are plotted as a function of the signal-to-noise ratio in Figure 4. If we assume that acceptable splitting errors are no more than $\delta t \pm 0.40$ s and $\phi \pm 20°$ the signal-to-noise level in the unfiltered data must be larger than 1.65. In contrast the polarization filter requires a minimum signal-to-noise level of 1.20. Thus filtering improves results for intermediate quality data (signal-to-noise level 1.20–2.00). On the basis of our experience, the *SKS* must be visible, albeit barely, on both the prefiltered radial and transverse components.

[18] Our splitting analysis not only estimates the splitting parameters, δt and ϕ, but also estimates the polarization of the shear wave before it enters the anisotropic region. In the case of *SKS* splitting this polarization should be close to the receiver-source back azimuth. An estimated source polarization significantly different from the back azimuth may indicate a polarization filter artifact. We impose the criterion that the estimated source polarization must be within 30° of the back azimuth for the splitting result to be acceptable.

[19] Our final condition for accepting a splitting result, after polarization filtering, is that the splitting is evident, but not necessarily well constrained, in the original unfiltered data. This further avoids fictitious splitting that may be an artifact of polarized noise.

4. Results

[20] After preprocessing 14 events were identified as being suitable for shear wave splitting analysis; these produced 34 measurements (Figure 1 and Tables 1 and 3). The results for MSEY are from *Barruol and Ben Ismail* [2001] and the results for RER are from *Behn et al.* [2004].

[21] The results show a regional pattern with coherent and smooth variations in polarization of the fast shear wave and significant variations in delay time. The main granitic Islands of Mahé, Praslin and surrounding islands show an average fast direction of ~30°, but a large variation in delay time (0.55–1.75 s). The outer islands show more variability in fast direction. The islands in the Amirantes show more north-south trends (ALPLB 12.9°) and the fast directions of the islands toward the Mascarene Plateau rotate in a clockwise sense (PLTPB 45.04°, CTVPS 69°). The delay

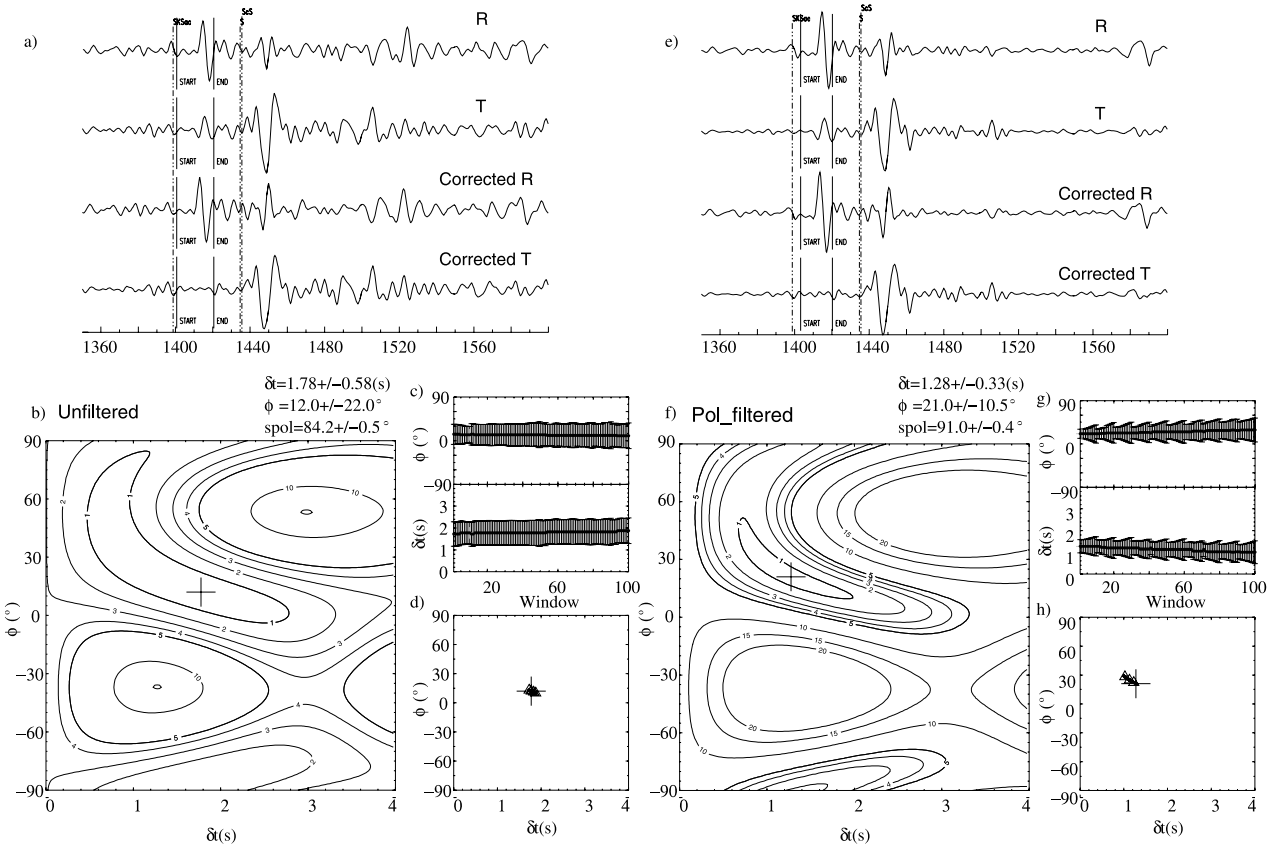

Figure 3. (a–d) Splitting analysis performed at MSEY on the event used in Figure 2 with microseismic noise of signal-to-noise ratio ~1.4 added. (e–h) Splitting analysis from the same data, after the use of polarization filters. See Figure 2 for definition of plots.

times for the Amirantes islands are relatively small (ALPLB 0.71 s) compared with the Mascarene Plateau (CTVPS 2.4 s, PLTPB 2.09 s).

5. Interpretations

5.1. Simple Asthenospheric Flow

[22] *Barruol and Ben Ismail* [2001] performed splitting analysis on the permanent IRIS station, MSEY. They found a fast shear wave polarization direction similar to those we have determined for the inner islands. They proposed that the anisotropy beneath the plateau is predominantly controlled by simple asthenospheric flow associated with African plate motion as predicted by the *Gripp and Gordon* [1990] model.

[23] More recent plate motion models show that the Seychelles are part of the smaller Somali plate, which moves quite differently from the larger African plate [*Kreemer et al.*, 2003]. Figure 1 shows the plate motion vector from the *Kreemer et al.* [2003] model, and Figure 5 shows the misfit between this plate motion and fast shear wave polarization. The plate motion direction only agrees with the observed fast direction at CTVPS (Coetivy). At many of the other stations the misfit is greater than 20°, with a total cumulative misfit for all stations of 590°. This suggests that LPO alignment of olivine by simple plate motion alone cannot explain the anisotropy beneath the Seychelles.

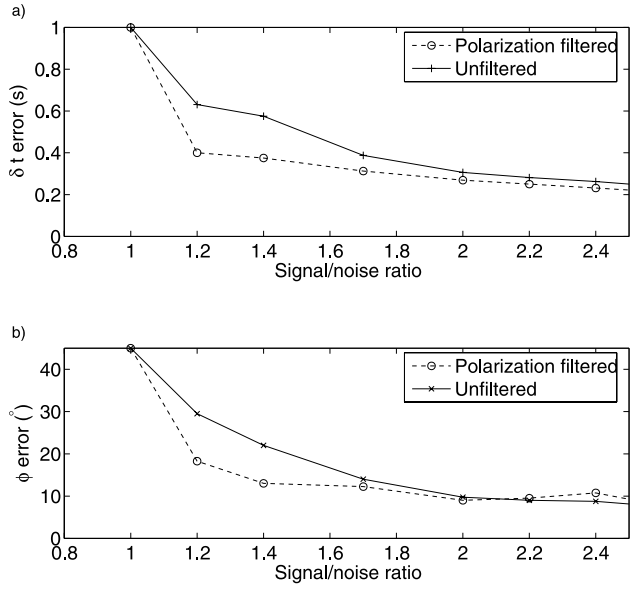

Figure 4. Error in splitting parameters, (a) δt and (b) fast direction, as a function of signal-to-noise ratio, before and after the application of polarization filters. Data will produce well constrained splitting results ($\delta t < 0.4$ s, $\phi <$ 20°) if the signal-to-noise ratio of the unfiltered data is larger than 1.65. In contrast, data after polarization filtering requires a signal-to-noise ratio of 1.20.

Table 3. Individual Shear Wave Splitting Measurements[a]

			Before Polarization Filter				After Polarization Filter				Average			
Station	Event	Phase	δt, s	δt Error, s	ϕ, deg	ϕ Error, deg	δt, s	δt Error, s	ϕ(°)	ϕ Error, deg	spol, deg	BAZ, deg	ϕ, deg	δt, s
ALPLB	5	*SKS*	0.45	0.28	−22	21.0	0.25	0.18	13.5	19.8	52.7	52.0		
ALPLB	7	*SKS*	0.85	0.16	14	14.8	0.93	0.16	9.5	8.0	75.8	92.3		
ALPLB	12	*SKS*	0.78	0.40	41	20.8	0.95	0.21	42.5	7.0	62.7	56.1	22	0.71
ARDPS	10	*SKS*	0.53	0.11	7	5.3	0.55	0.18	14.3	14.2	29.0	48.0	14	0.55
BRDPS	4	*SKKS*	0.33	0.95	62	26.8	0.53	0.22	18.0	18.0	92.7	96.6	18	0.53
CRSPS	2	*SKS*	0.90	0.05	76	6.0	0.90	0.07	45.0	7.3	109.9	125.5		
CRSPS	10	*SKKS*	0.83	0.24	54	16.5	0.85	0.21	35.0	12.0	74.5	48.0	40	0.88
CTVPS	3	*SKS*	2.00	0.21	90	14.5	2.05	0.20	81.1	9.5	106.6	116.3		
CTVPS	9	*SKS*	2.63	0.51	54	7.0	2.78	0.04	57.1	5.8	206.4	187.0	69	2.41
DNSPB	4	*SKS*	0.75	0.11	41	7.3	0.78	0.11	46.0	7.8	100.7	96.5	46	0.78
DSRPS	1	*SKS*	1.00	0.17	31	14.0	1.03	0.09	32.4	7.5	91.2	123.1	32	1.03
FLCPS	4	*SKS*	0.90	0.10	19	9.5	0.83	0.12	14.8	9.0	68.4	96.6	15	0.83
LDGPS	10	*SKKS*	1.08	0.84	39	15.8	0.95	0.18	29.9	9.3	54.5	48.0	30	0.95
MHDLB	4	*SKS*	1.03	0.44	18	12.8	0.90	0.27	25.3	8.8	100.2	96.6		
MHDLB	5	*SKS*	0.83	0.03	11	5.3	0.95	0.04	27.3	3.5	58.8	51.7	26	0.93
MHNPS	8	*SKS*	1.65	0.33	44	5.8	1.80	0.29	45.4	4.3	55.2	42.7		
MHNPS	10	*SKKS*	0.88	0.08	18	8.3	0.93	0.07	25.4	5.8	55.4	48.0	35	1.37
MHPLB	6	*SKS*	1.40	0.56	36	17.5	1.75	0.36	30.4	7.0	97.2	95.7	30	1.75
MHSPS	10	*SKKS*	1.23	0.09	20	4.5	1.23	0.16	22.7	8.5	46.7	48.0		
MHSPS	12	*SKS*	1.15	0.11	16	6.8	1.20	0.15	20.7	8.5	51.2	55.9	22	1.21
MMLPS	10	*SKKS*	0.95	0.33	16	23.8	0.90	0.21	18.5	11.3	36.1	48.0		
MMLPS	12	*SKS*	1.23	0.04	34	2.3	1.23	0.06	40.5	5.3	66.2	55.9	29	1.06
NRDPS	10	*SKKS*	1.00	0.08	24	3.5	1.00	0.11	34.1	4.8	45.7	48.0	34	1.00
PRTLB	4	*SKS*	1.00	0.35	25	13.0	0.90	0.29	27.5	13.3	100.2	96.6		
PRTLB	8	*SKS*	0.98	0.28	34	8.8	0.85	0.24	31.5	7.0	48.3	42.7		
PRTLB	11	*SKS*	1.08	0.23	46	13.8	1.08	0.26	43.5	16.3	93.7	96.1	34	0.94
SLHLB	4	*SKS*	0.75	0.21	37	11.5	0.88	0.18	31.1	7.5	102.4	96.6		
SLHLB	10	*SKKS*	1.00	0.14	20	5.8	0.98	0.21	15.1	7.5	45.5	48.0		
SLHLB	13	*SKS*	0.88	0.13	40	10.3	0.83	0.13	40.1	12.3	98.2	95.9		
SLHLB	14	*SKS*	1.40	0.65	44	23.5	1.25	0.17	56.1	9.8	122.5	115.2	35	0.98

[a]Measurements before and after the application of polarization filters are shown. Average splitting results are calculated from the postpolarization filtered results. BAZ, back azimuth; spol, the source polarization (the polarization of the shear wave before it enters the anisotropic medium).

5.2. Effect of the African Superswell

[24] *Behn et al.* [2004] studied the effect of the African superswell on large-scale mantle flow around Africa, taking into account density-driven flow due to mantle heterogeneity and plate motion. Plate motion is represented in their model by calculating the instantaneous flow field due to global plate motions on a reference viscosity structure. Additionally they calculate mantle flow associated with internal density variations, using S20RTS, the global shear wave tomography model of *Ritsema et al.* [1999]. The contribution from each of these mechanisms is controlled with a viscosity scale factor ($0 < \beta < 1$, $\beta = 0$ is the case for density-driven flow only, and $\beta = 1$ is the case for simple asthenospheric flow (SAF)). Strain rates caused by plate motion flow are independent of mantle viscosity structure; however, strain rates caused by density-driven flow are inversely proportional to the mantle viscosity structure [*Behn et al.*, 2004]. The viscosity scale factor is multiplied with the reference viscosity structure for the mantle and the resulting plate motion and density-driven flow models are summed.

[25] They found that shear wave splitting measurements from the circum-African stations agreed best with their model when mantle flow was influenced by both density-driven flow and plate motions ($\beta = 0.35$). This model shows poor agreement with our shear wave splitting results for the Seychelles (Figure 6). Reducing the asthenospheric viscosity ($\beta = 0.2$), so that the flow is influenced more by density-driven flow, provides a better fit (Figure 6), reducing the misfit from 272° to 245°. Therefore reconciling our results

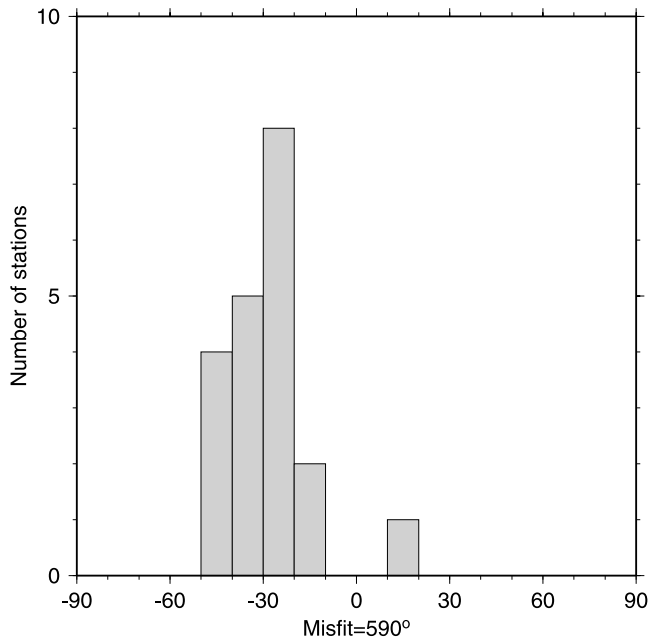

Figure 5. Histogram showing the relative misfit between plate motion orientation [*Kreemer et al.*, 2003] and observed shear wave splitting fast direction. The large misfits show that a simple plate motion model poorly explains the results.

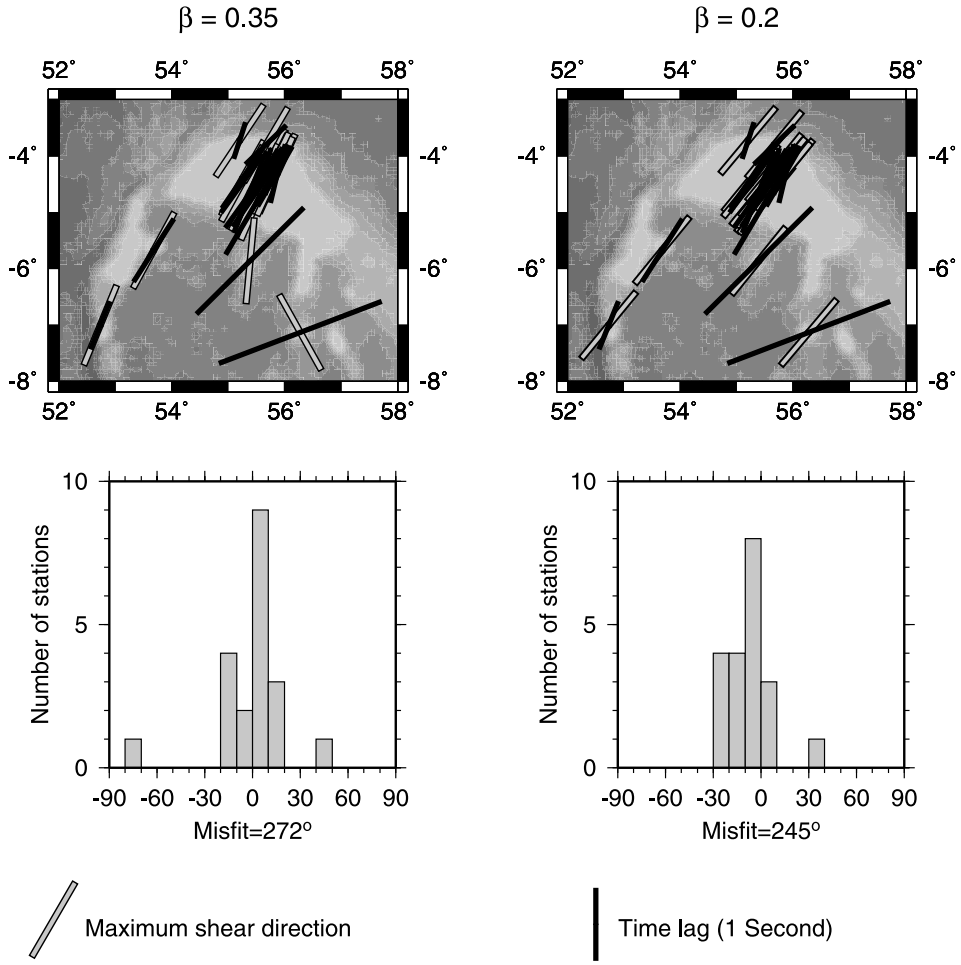

Figure 6. Comparison between maximum shear direction calculated due to large-scale flow associated with the upwelling African superplume and plate motion (left) for the preferred model of *Behn et al.* [2004] ($\beta = 0.35$) and (right) for a model with a larger component of density-driven flow ($\beta = 0.2$) and observed shear wave splitting fast direction. Open lines show the direction of maximum shear and those shown in the top left plot are the same as those in Figure 4c from *Behn et al.* [2004]. Solid lines show fast directions calculated in this study. Relative misfit between maximum shear direction and observed shear wave splitting fast direction for (left) $\beta = 0.35$ and (right) $\beta = 0.2$. The better fit with the $\beta = 0.2$ model implies a significant laterally varying viscosity structure in the mantle beneath the Indian Ocean.

from the Seychelles with the other circum-African stations would require significant lateral variation in viscosity, and hence imply that the influence of the density-driven flow is also variable.

5.3. Plume Hypothesis

[26] *Montelli et al.* [2004] used finite frequency tomography to image a plume-like feature impinging on the Earth's surface at 56°E, 6°S, directly beneath the Seychelles Plateau. Flow in the mantle associated with this plume could provide a plausible mechanism for anisotropy. *Ribe and Christensen* [1994] numerically modelled asthenospheric flow beneath Hawaii. They showed an approximately parabolic flow pattern due to a plume impinging on a moving plate. Following the method described by *Milne-Thomson* [1968] and similar to studies by *Sleep* [1990], *Savage and Sheehan* [2000], and *Walker et al.* [2001], we approximate this flow using a point source approximation where the plume impinges on the Earth's surface and determine the stream functions associated with the radial flow of the buoyant material into a horizontal flow field. We then perform a grid search over two of the three parameters that constrain the flow field: plume center (latitude, longitude) and parabolic width, P ($P = M/S$, where M is plume strength [m^2 s] and S is plate velocity [m/s]). Plate velocity is taken from the *Kreemer et al.* [2003] plate motion models, so P depends solely on the plume strength. The fourth parameter, direction of plate motion, is constrained by the *Kreemer et al.* [2003] plate motion models and has an orientation of 59°.

[27] Figure 7 shows streamlines from a model with plume centered at 56.3°E, 5.1°S and $P = 50$ km. Plume centers, their associated 95% F test confidence regions and misfit plots are shown for three models of varying P, where P is a ratio between plume strength and plate velocity. For large values of P the resultant flow is dominated by the radial plume flow. As the plume center is unconstrained, it is easy to fit models which are dominated by radial flow for a

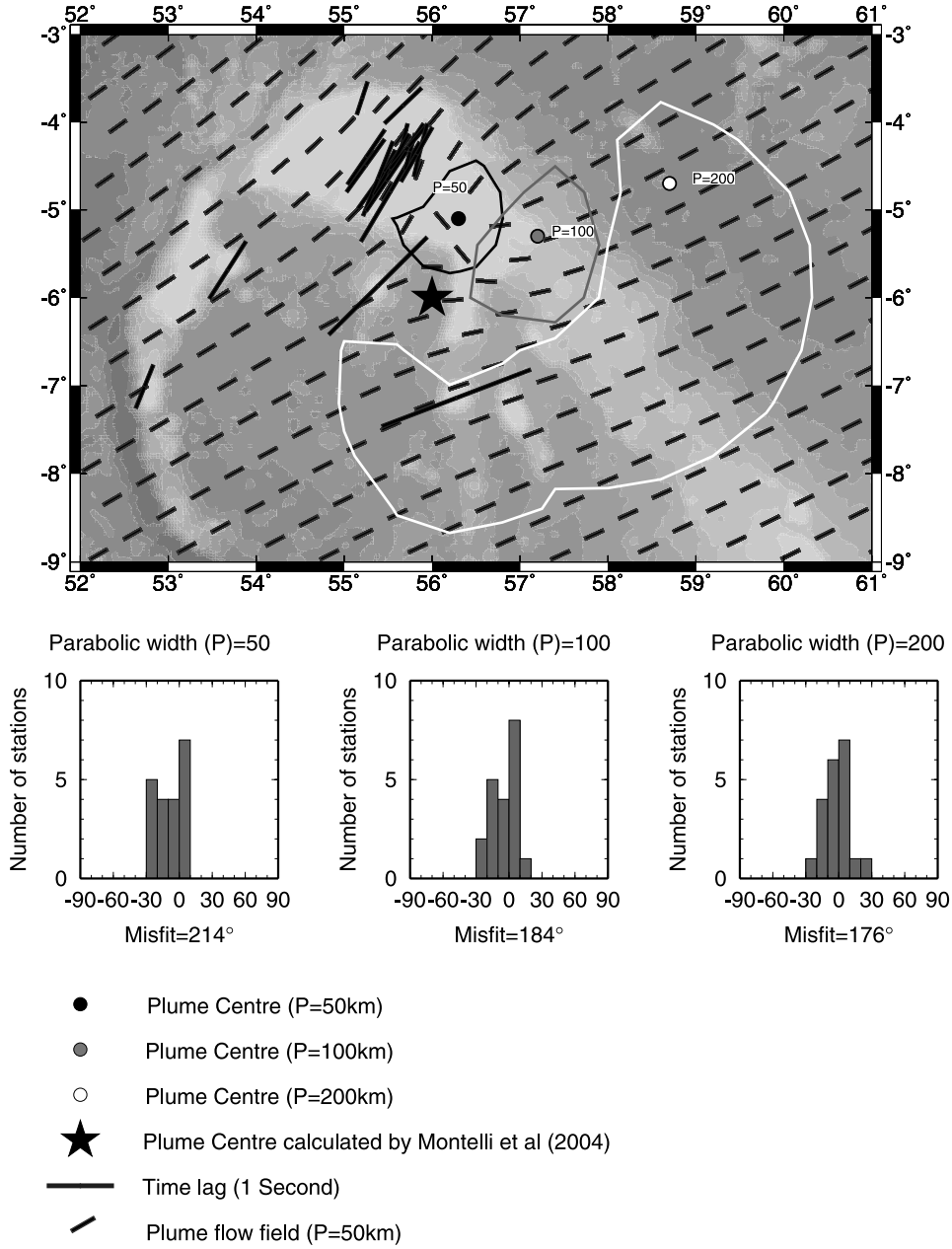

Figure 7. (top) Comparison between expected plume flow due to plume centered at 56.3°E, 5.1°S and parabolic width (P) 50 km and observed shear wave splitting parameters. Also shown are the best fit plume locations for models with P = 50 km, P = 100 km and P = 200 km with their estimated 95% confidence region (bold contours). The star indicates the plume center as found by *Montelli et al.* [2004]. Relative misfit between plume flow and observed shear wave splitting fast direction for (bottom left) P = 50 km, (bottom middle) P = 100 km, and (bottom right) P = 200 km. As P increases, the misfit is reduced but the plume location is much less well constrained.

variety of plume centers. This is evidenced in our models by the misfit reducing and errors increasing for the best fitting plume centers, out to a parabolic width of 200 km and beyond (Figure 7). *Walker et al.* [2001] calculate a best fitting parabolic flow model at Hawaii to have P = 200 km. We find that such a parabolic width can explain well the majority of the shear wave splitting results at the Seychelles (misfit 176°, ALPLB 26.2° and BRDPS 20.1° are the exceptions). However, the plume center for this model lies well off the Seychelles plateau, where there is no other evidence of an upwelling the size of that beneath Hawaii (e.g., gravity [*Reigber et al.*, 2005]). This suggests that a more likely case is a smaller plume located beneath the plateau where such evidence could be hidden by the continental crust, especially if the plume is incipient. This is shown in Figure 7, where a model with P = 50 km is constrained to be beneath the plateau, ~100 km from the location determined by *Montelli et al.* [2004], but the misfit is slightly worse than that for the larger plume model (misfit 214° and ALPLB, ARDPS, BRDPS, DSRPS, and FLCPS

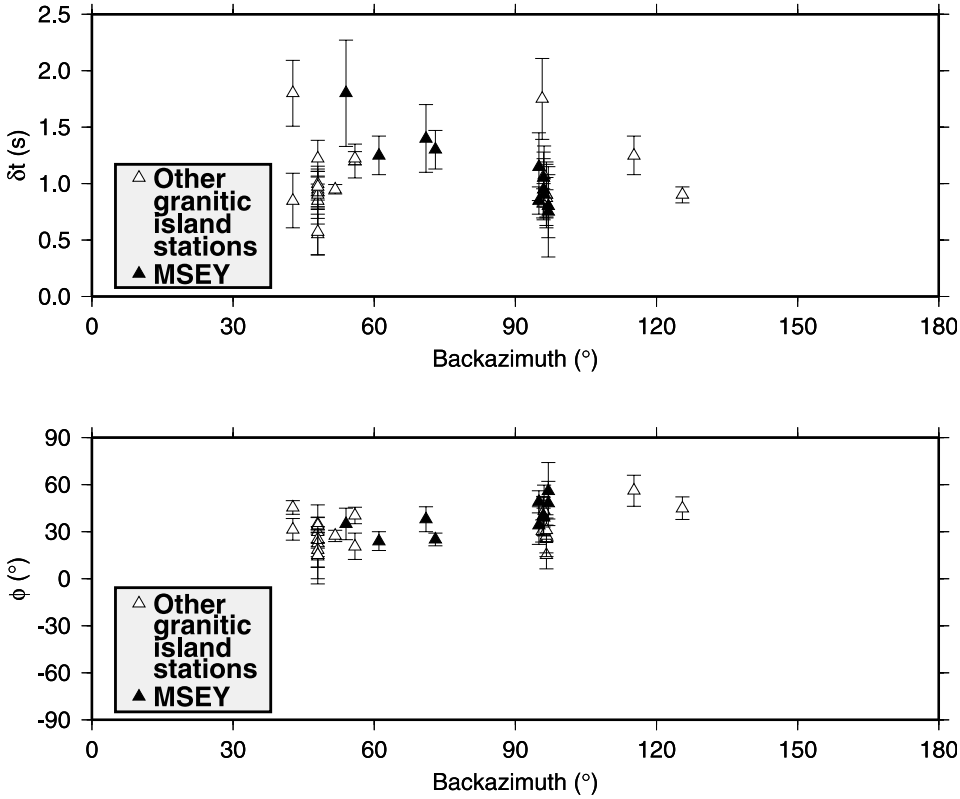

Figure 8. Anisotropy parameters, (top) δt and (bottom) fast direction ϕ, as a function of back azimuth. The large variation in δt with back azimuth shows that a significant lithospheric component must be present; however, the variation of ϕ with back azimuth is small.

have misfits larger than 20°). In the real data the magnitude of the shear wave splitting results increase with proximity to the hypothesized plume source. This is perhaps as expected: the strongest anisotropy is present in the area where shear is highest due to the opposing flows of the northeast plate motion and southwest plume-driven flow. The geographic coverage of stations is a bit limited to fully test this model as all measurements of anisotropy are situated west of the modeled plume center.

5.4. Fossil Anisotropy

[28] The large variation in time lag over the small spatial area of the main granitic islands strongly suggests a lithospheric component of anisotropy. Hence two layers of anisotropy might be expected, a contribution from the lithosphere and one from the underlying mantle. Variations in shear wave splitting parameters with back azimuth can indicate vertical variation in anisotropy [e.g., *Silver and Savage* 1994] or lateral variations in mantle velocity structure. Figure 8 displays the anisotropy parameters from MSEY [*Barruol and Ben Ismail*, 2001] and the main granitic islands as a function of back azimuth. There is little variation in fast direction and no systematic variation in delay times in either MSEY or the main granitic islands. This suggests a single layer of anisotropy is present across the Seychelles plateau; however, the large lag times and their variability suggest that either this layer is not constant in thickness or that the magnitude of the anisotropy is variable across the region. The large amounts of splitting beneath the Mascarene Plateau (e.g., 2.4 s at CTVPS) might suggest an additional asthenospheric component.

[29] It has been proposed that the Amirantes ridge/trough complex, where Alphonse (ALPLB) and Desroche (DSRPS) are found, is a result of volcanic activity induced along a transform fault where the Seychelles/India plate rubbed against the Somali plate [*Plummer*, 1996] (Figure 1). Fast directions in the Amirantes and the granitic islands are parallel to the location of this fault, suggesting that this has led to a fossil anisotropy to be frozen in to the lithosphere. Stations further from the transform fault (CTVPS 69°, PLTPB 45°) show fast directions more similar to plate motion (~60°). The distance from the fault and the fact that these stations are on the edge of the Seychelles plateau, and could have a thinner lithosphere, suggest that the rotation observed in our results is due to more than one mechanism being present across the area. Where the lithosphere is thick past tectonic episodes dominate the anisotropic signature. In contrast where the lithosphere is thinner, deeper mantle processes, such as asthenospheric flow, play a larger role.

6. Conclusions

[30] Teleseismic data from an array of temporary stations deployed across the Seychelles have been used to study upper mantle anisotropy beneath the region. Data preprocessing included component realignment and polarization filtering. Principal component analysis (PCA) of *P* waves was used to estimate the alignment corrections. Polarization

Table 4. Relative Misfits[a]

Anisotropy Mechanism	Misfit, deg
Plate motion	590
Large-scale mantle flow for $\beta = 0.35$	272
Large-scale mantle flow for $\beta = 0.20$	245
Plume hypothesis for $P = 200$ km	176
Plume hypothesis for $P = 100$ km	184
Plume hypothesis for $P = 50$ km	214

[a]Misfits from all the models calculated in this study are shown. Misfits are cumulative differences between shear wave splitting fast direction and predicted flow direction from model for each station.

filters can significantly improve the signal-to-noise ratio of seismograms. Such filters are ideal for noisy, temporary networks, especially those on oceanic islands where microseismic noise is large. We have developed the following criteria for the use of such filters with the analysis of *SKS*/*SKKS* splitting:

[31] 1. The *SKS* signal must be evident on both the radial and transverse components. Tests show that in prefiltered data a signal (*SKS*) to noise ratio of 1.2 must be observed on the weakest component.

[32] 2. The estimated *SKS* polarization before entering the anisotropic region must be within 30° of the receiver-source great circle path.

[33] 3. The splitting analysis must produce a consistent result before and after the application of the polarization filters. In general, the filtering improves the errors and hence confidence in the results. This reduces the risk of obtaining a fictitious result from polarized noise.

[34] The shear wave splitting results show a significant amount of anisotropy beneath the Seychelles, with large variations in both, the magnitude of splitting (δt), and, the fast shear wave polarization direction (ϕ). However, there is little evidence for vertical variations in the orientation of the anisotropy. Table 4 shows misfits from all the models proposed in this paper. It is evident that simple asthenospheric flow has a large misfit and cannot explain lateral variations in the data. All other models offer similar misfits and are plausible models to explain the observed anisotropy. A combination of plate motion and large-scale density-driven flow may explain a component of the observed anisotropy. Thermal upwelling associated with the African superswell can explain the results better if there are significant lateral variations in the viscosity structure of the mantle in the region. Alternatively, a focused mantle plume, as suggested in a recent tomographic model [*Montelli et al.*, 2004], can also explain the pattern of splitting and the misfit suggests that this model fits better than the other models tested although the model is limited by the geographic cover of the stations and the number of free parameters involved. However, the large variation in δt over a small area suggests that a lithospheric component must be present beneath the Seychelles plateau. Transpressive deformation is likely to be the primary cause of anisotropy close to the Amirante ridge/trough system, with simple asthenospheric flow becoming more dominant moving further from this area of major faulting and off the plateau. Constraints from other techniques such as receiver functions and regional travel time tomography should help better discriminate between these models.

[35] **Acknowledgments.** We would like to thank Mark Behn for calculating various mantle flow models, Weijan Mao for supplying the polarization filters, and Matt Evans for the program that calculates plate motion. GEOFON is acknowledged for archiving data from the experiment, and IRIS is acknowledged for the MSEY data. Jenny Collier, Tim Minshull, Bob Whitmarsh, Patrick Samson, Albrecht Schulze, and Jen Caddick are thanked for help with the experiment. Considerable logistic support came from many people, companies, and government agencies in the Seychelles. In particular, we would like to thank Seychelles Centre Marine Research Technology (Evariste Michel and Jude Bijoux), Island Development Committee (Justin Moustache), Marine Parks Authority, Ministry of Tourism (Eddie Belle), Ministry of Environment (Rolph Payet and Victorin Laboudallon), Gondwana Granite (Selwyn Gendron), Seychelles Marketing Board and Seychelles Island Foundation, and the managers/owners of the following islands: Bird, Denis, Aride, Cousine, Felicite, La Digue, Silhouette, Île du Nord, Coetivy, Île Platte, Desroche, and Alphonse. The instrument pool of GeoForschungsZentrum Potsdam is thanked for providing seismic stations. Funding was provided by the Natural Environmental Research Council (NERC), grant NER/A/S/2000/01390, the Royal Society, grant RSRG 24044, and the GeoForschungsZentrum Potsdam.

References

Babuska, V., and M. Cara (1991), *Seismic Anisotropy in the Earth*, 217 pp., Springer, New York.

Barruol, G., and W. Ben Ismail (2001), Upper mantle anisotropy beneath the African IRIS and GEOSCOPE stations, *Geophys. J. Int.*, *146*, 549–561.

Behn, M. D., C. P. Conrad, and P. G. Silver (2004), Detection of upper mantle flow associated with the African Superplume, *Earth Planet. Sci. Lett.*, *224*, 259–274.

Collier, J. S., et al. (2004), Rapid continental breakup and microcontinent formation in the western Indian Ocean, *Eos Trans. AGU*, *85*(46), 481, 487.

Debayle, E., B. Kennett, and K. Priestley (2005), Global azimuthal seismic anisotropy and the unique plate-motion deformation of Australia, *Nature*, *433*, 509–512.

Du, Z., G. R. Foulger, and W. Mao (2000), Noise reduction for broad-band, three-component seismograms using data–adaptive polarization filters, *Geophys. J. Int.*, *141*, 820–828.

Duncan, R. A., and D. G. Pyle (1988), Rapid eruption of the Deccan flood basalts at the Cretaceous/Tertiary boundary, *Nature*, *333*, 841–843.

Gaina, C., R. D. Müller, B. Brown, and T. Ishihara (2003), Microcontinent formation around Australia, in *The Evolution and Dynamics of the Australian Plate*, *Spec. Pap. Geol. Soc. Am.*, *372*, 405–416.

Gripp, A. E., and R. G. Gordon (1990), Current plate velocities relative to the hotspots incorporating the NUVEL-1 global plate motion model, *Geophys. Res. Lett.*, *17*, 1109–1112.

Gung, Y., M. Panning, and B. Romanowicz (2003), Global anisotropy and the thickness of continents, *Nature*, *422*, 707–711.

Hastings, D. A., and P. K. Dunbar (1999), Global land one-kilometer base elevation (GLOBE) Digital Elevation Model, documentation, vol. 1.0, Key to Geophysical Records Documentation KGRD 34, NOAA, Natl. Geophys. Data Cent., Boulder, Colo.

Karato, S. (1992), On the Lehmann discontinuity, *Geophys. Res. Lett.*, *19*, 2255–2258.

Kreemer, C., W. E. Holt, and A. J. Haines (2003), An integrated global model of present-day plate motions and plate boundary deformation, *Geophys. J. Int.*, *154*, 8–34.

Mainprice, D., G. Barruol, and W. Ben Ismail (2000), The seismic anisotropy of the Earth's mantle: From single crystal to polycrystal, in *Earth's Deep Interior: Mineral Physics and Tomography From the Atomic to the Global Scale*, *Geophys. Monogr. Ser.*, vol. 117, 237–264, AGU, Washington, D.C.

Mainprice, D., A. Tommasi, H. Couvy, P. Cordier, and D. J. Frost (2005), Pressure sensitivity of olivine slip systems and seismic anisotropy of Earth's upper mantle, *Nature*, *433*, 731–733.

McCall, R. A. (1997), Implications of recent geological investigations of the Mozambique channel for the mammalian colonization of Madagascar, *Proc. R. Soc. London, Ser. A*, *264*, 663–665.

Miller, J. A., and J. D. Mudie (1961), Potassium–argon age determinations on granite from the islands of Mahé in the Seychelles archipelago, *Nature*, *192*, 1174–1175.

Milne-Thomson, L. M. (1968), *Theoretical Hydrodynamics*, 5th ed., 743 pp., Macmillan, New York.

Montelli, R., G. Nolet, F. A. Dahlen, G. Masters, E. R. Engdahl, and S. Hung (2004), Finite–frequency tomography reveals a variety of plumes in the mantle, *Science*, *303*, 338–343.

Müller, R. D., W. R. Roest, J. Royer, L. M. Gahagan, and J. G. Sclater (1997), Digital isochrons of the world's ocean floor, *J. Geophys. Res.*, *102*, 3211–3214.

Müller, R. D., C. Gaina, W. R. Roest, and D. L. Hansen (2001), A recipe for microcontinent formation, *Geology*, *29*(3), 203–206.

Park, J., F. L. Vernon, and C. R. Lindberg (1987), Frequency dependent polarization analysis of high–frequency seismograms, *J. Geophys. Res.*, *92*, 12,664–12,674.

Plummer, P. S. (1995), Ages and geological significance of the igneous rocks from Seychelles, *J. Afr. Earth. Sci*, *20*, 91–101.

Plummer, P. S. (1996), The Amirante ridge/trough complex: Response to rotational transform rift/drift between Seychelles and Madagascar, *Terra Nova*, *8*, 34–47.

Plummer, P. S., and E. R. Belle (1995), Mesozoic tectono-stratigraphic evolution of the Seychelles microcontinent, *Sediment. Geol.*, *96*, 73–91.

Reading, A. M., W. Mao, and D. Gubbins (2001), Polarization filtering for automatic picking of seismic data and improved converted phase detection, *Geophys. J. Int.*, *147*, 227–234.

Reigber, C., et al. (2005), A high resolution global gravity field model combining CHAMP and GRACE satellite mission and surface gravity data: EIGEN-CG01C, *J. Geod*, in press.

Ribe, N. M., and U. R. Christensen (1994), Three–dimensional modeling of plume-lithosphere interaction, *J. Geophys. Res.*, *99*, 669–682.

Ritsema, J., H. J. van Heijst, and J. H. Woodhouse (1999), Complex shear wave velocity structure imaged beneath Africa and Iceland, *Science*, *286*, 1925–1928.

Savage, M. K., and A. T. Sheehan (2000), Seismic anisotropy and mantle flow from the Great Basin to the Great Plains, western United States, *J. Geophys. Res.*, *105*, 13,715–13,734.

Schlich, R. (1982), The Indian Ocean: Aseismic ridges, spreading centres and basins, in *The Ocean Basins and Margins*, vol 6, *The Indian Ocean*, pp. 51–147, Springer, New York.

Schulte-Pelkum, V., P. S. Earle, and F. L. Vernon (2004), Strong directivity of ocean-generated seismic noise, *Geochem. Geophys. Geosyst.*, *5*(3), Q03004, doi:10.1029/2003GC000520.

Silver, P. G., and W. W. J. Chan (1991), Shear wave splitting and subcontinental mantle deformation, *J. Geophys. Res.*, *96*, 16,429–16,454.

Silver, P. G., and M. K. Savage (1994), The interpretation of shear wave splitting parameters in the presence of two anisotropic layers, *Geophys. J. Int.*, *119*, 949–963.

Sleep, N. H. (1990), Hotspots and mantle plumes: some phenomenology, *J. Geophys. Res.*, *95*, 6715–6736.

Smith, W. H. F., and D. T. Sandwell (1997), Global sea floor topography from satellite altimetry and ship depth soundings, *Science*, *277*, 1956–1962.

Teanby, N. A., J.-M. Kendall, and M. Van der Baan (2004), Automation of shear-wave splitting measurements using cluster analysis, *Bull. Seismol. Soc. Am.*, *94*(2), 453–463.

Tucker, R. D., L. D. Ashwal, and T. H. Torsvik (2001), U–Pb geochronology of Seychelles granitoids: A Neoproterozoic continental arc fragment, *Earth Planet. Sci. Lett.*, *187*, 27–38.

Walker, K. T., G. H. R. Bokelmann, and S. L. Klemperer (2001), Shear-wave splitting to test mantle deformation models around Hawaii, *Geophys. Res. Lett.*, *28*(22), 4319–4322.

Walsh, R. P. D. (1984), Climate of the Seychelles, in *Biogeography and Ecology of the Seychelles Islands*, pp. 39–62, Springer, New York.

Wasserburg, G. J., H. Craig, H. W. Menard, A. E. J. Engel, and C. J. Engel (1963), Age and composition of a Bounty Islands granite and age of a Seychelles Islands granite, *J. Geol.*, *71*, 785–789.

Wegener, A. (1924), *The Origin of Continents and Oceans*, 212 pp., Methuen, New York.

Wookey, J., and J. Kendall (2004), Evidence of midmantle anisotropy from shear wave splitting and the influence of shear-coupled *p* waves, *J. Geophys. Res.*, *109*, B07309, doi:10.1029/2003JB002871.

J. O. S. Hammond and G. Stuart, School of Earth and Environment, Earth Science, University of Leeds, Leeds LS2 9JT, UK. (j.hammond@earth.leeds.ac.uk)

P. Joseph, Seychelles National Oil Company, Victoria, Mahé, Seychelles.

J.-M. Kendall and J. Wookey, Department of Earth Sciences, University of Bristol, Wills Memorial Building, Queens Road, Bristol BS8 1RJ, UK.

G. Rümpker, Arbeitsbereich Geophysik, Johann Wolfgang Goethe-Universitat, Feldbergstr. 47, D-60323 Frankfurt am Main, Germany.

T. Ryberg, Potsdam, Telegrafenberg, D-14473 Potsdam, Germany.

N. Teanby, Atmospheric, Oceanic and Planetary Physics, University of Oxford, Clarendon Laboratory, Parks Road, Oxford OX1 3PU, UK.